frontiers in Materials

ORIGINAL RESEARCH
published: 09 January 2020
doi: 10.3389/fmats.2019.00337

Green and Low-Cost Membrane Electrode Assembly for Proton Exchange Membrane Fuel Cells: Effect of Double-Layer Electrodes and Gas Diffusion Layer

M. H. Gouda[1], *Mohamed Elnouby*[2], *Andrew N. Aziz*[3], *M. Elsayed Youssef*[3], *D. M. F. Santos*[4*] *and Noha A. Elessawy*[5*]

[1] *Polymer Materials Research Department, Advanced Technology and New Materials Research Institute, City of Scientific Research and Technological Applications, New Borg El-Arab City, Egypt,* [2] *Nanomaterials and Composites Research Department, Advanced Technology and New Materials Research Institute, City of Scientific Research and Technological Applications, New Borg El-Arab City, Egypt,* [3] *Computer Based Engineering Applications Department, Informatics Research Institute IRI, City of Scientific Research and Technological Applications, New Borg Al-Arab City, Egypt,* [4] *Center of Physics and Engineering of Advanced Materials, Instituto Superior Técnico, Universidade de Lisboa, Lisbon, Portugal,* [5] *Advanced Technology and New Materials Research Institute, City of Scientific Research and Technological Applications, New Borg Al-Arab City, Egypt*

OPEN ACCESS

Edited by:
M. Jasim Uddin,
University of Texas Rio Grande Valley Edinburg, United States

Reviewed by:
Qihui Wu,
Jimei University, China
Muhammad Zobayer Bin Mukhlish,
Shahjalal University of Science and Technology, Bangladesh

****Correspondence:***
D. M. F. Santos
diogosantos@tecnico.ulisboa.pt
Noha A. Elessawy
nony_essawy@yahoo.com

Specialty section:
This article was submitted to Carbon-Based Materials, a section of the journal Frontiers in Materials

Received: *29 September 2019*
Accepted: *06 December 2019*
Published: *09 January 2020*

Citation:
Gouda MH, Elnouby M, Aziz AN, Youssef ME, Santos DMF and Elessawy NA (2020) Green and Low-Cost Membrane Electrode Assembly for Proton Exchange Membrane Fuel Cells: Effect of Double-Layer Electrodes and Gas Diffusion Layer. Front. Mater. 6:337. doi: 10.3389/fmats.2019.00337

The success of fuel cells depends on the proper design of the electrodes and membrane allowing easy access of oxygen and protons. Using non-precious catalyst electrodes based on recyclable carbon nanostructures is most important to produce clean energy and increase the ability to commercialize the fuel cells. Herein, reduced graphene oxide (rGO) and graphene/magnetic iron oxide nanocomposite (rGO/MIO) are successfully synthesized as anode and cathode, respectively, from polyethylene terephthalate (PET) waste bottles using easy steps in order to simplify the method and reducing the production cost. While, the membrane is prepared from low cost and eco-friendly ternary polymers blend which are polyvinyl alcohol (PVA), polyethylene oxide (PEO) and polyvinyl pyrrolidone (PVP) then doped with sulfonated graphene oxide. The prepared electrodes have characteristic high porosity and their electrocatalytic performances are evaluated using three-electrode cell electrochemical studies as cyclic voltammetry and linear scan voltammetry combined with rotating disk electrode. A new assembly of the membrane between two non-precious catalyst electrodes as a single polymer electrolyte membrane fuel cell (PEMFC) was developed using a catalyst-coated membrane technique. The membrane electrode assembly (MEA) design parameters which affect its performance in hydrogen fuel cells as number of used catalyst layers (CL) or using gas diffusion layer (GDL) were evaluated in a single cell set-up with H_2/O_2 operation and the results revealed that the performance MEA was enhanced with using GDL more than that of MEA without GDL by 66% at a current density of 0.8 A cm^{-2} while the performance with double CL was better than that of the conventional single CL by 30% at a current density of 0.98 mA cm^{-2}.

Keywords: graphene, graphene iron oxide composites, proton exchange membrane, membrane electrode assembly, hydrogen fuel cells

INTRODUCTION

As a result of the rapid urbanization since the beginning of the last century, the global growth of fossil fuel energy consumption has increased, leading to an increase in environmental pollution rate. Consequently, environmental pollution has shifted research attention to get clean energy conversion and storage systems. Fuel cells are known as one of the cleanest energy conversion systems due to their high energy density, high energy-conversion efficiency, environmental safety, and other outstanding features (Frey and Linardi, 2004).

Among different types of fuel cells, the polymer electrolyte membrane fuel cell (PEMFC) is a promising green energy conversion technology for both portable and stationary devices, as well as transportation applications. This is may be due to its economic, high efficiency, low-temperature operation, zero or low emission and rapid start-up (Gouda et al., 2019). The conversion process of chemical to electrical energy in PEMFCs depends on two chemical reactions at anode and cathode where oxygen reduction occurs at the cathode and hydrogen oxidation occurs at the anode (Liu et al., 2019a) and both reactions need catalysts to reduce the electrochemical over-potential and to increase the voltage output. The oxygen reduction reaction (ORR) at the cathode is a multistep reaction involved with multielectron, thus the ORR reaction consumes most of the catalyst material. Consequently, the development of low cost, high-performance electrocatalysts for improving ORR kinetics is essential to reduce the cost of PEMFCs (Liu et al., 2019b). Pt-based composites are considered as the most efficient cathode catalysts, but they have disadvantages as high cost, crossover poisoning and low stability especially in acidic media (Choi et al., 2015). However, high-performance non-precious metal catalysts (NPMCs) simultaneously active for the ORR at the cathode and the hydrogen oxidation reaction (HOR) at the anode are desperately needed to replace these precious metals and to solve the drawbacks (Gupta et al., 2016). Under these circumstances, transition metal oxides (Gao et al., 2017; Lai et al., 2017), hybrid inorganic nanocarbon materials (Su et al., 2014; Ye et al., 2017) and carbon-doped metal-free heteroatom nanomaterials (Dumont et al., 2019) were used to substitute platinum for constructing highly efficient non-precious metal catalysts. Where, the promoted activity of doped carbon materials may be attributed to the electron-donating or electron-accepting behavior between adjacent carbon atoms and the heteroatoms, which modify the charge allocation in the carbon plane (Shen et al., 2014).

In addition to catalyst electrodes, the polymeric proton exchange membrane is one of the most important components of PEMFCs. Thus, development of the proton exchange membrane using non-perfluorinated based polymers as new alternative membranes attracted many researchers with the aim of replacing benchmark Nafion® membranes to reduce the production cost and to be closer to commercialization (Bakangura et al., 2016; Pourzare et al., 2016). However, the non-perfluorinated based polymers are usually modified chemically with several treatments, such as polymers blending, incorporation of doping agents in the polymer matrix as carbon-based nanomaterials and polymers sulfonation to improving the membrane properties (Awang et al., 2015; Pourzare et al., 2016; Sedesheva et al., 2016; Pandey et al., 2017).

Recently, graphene (G) and graphene-based materials have received great interest as a promising material for fuel cell applications due to its remarkable advantages, such as; large specific surface area, mechanical flexibility, and good electrical conductivity. In particular, a significant improvement in the electrocatalytic activity of electrodes was observed with graphene or modified graphene as the catalyst support or as a metal-free catalyst (Iwan et al., 2015; Morales-Acosta et al., 2019). Moreover, the incorporation of graphene oxide (GO) or sulfonated graphene oxide (SGO) into a polymer matrix of the PEM (Li et al., 2017; Pandey et al., 2017; Qiu et al., 2017) enhance its ionic conductivity and improve its physicochemical properties (Beydaghi et al., 2014).

In recent years, many researchers have been interested in turning the membrane electrode assembly (MEA) prototypes into commercially valuable products by improving its overall efficiency, increase current density and decrease the cost of the membrane and catalytic materials used. However, the results show that the true performance of the MEA for PEMFC is not only depended on the properties of the individual components but also depend on the MEA production method and the operating conditions in the cell (Aziz et al., 2018) such as the composition of electrode inks, electrode pressing, percentage of humidification and applied pressure on both electrodes, gas diffusion layer (GDL) materials used and cell temperature (Frey and Linardi, 2004; Thanasilp and Hunsom, 2010; Kim et al., 2015).

Motivated by these observations, this research concerns the production of low-cost MEA for PEMFC using non-precious metal graphene-based materials as catalytic electrodes prepared from the thermal dissociation of plastic waste using simple, one-pot, environmentally-friendly, and applicable synthesis method. While the polymeric proton exchange membrane was produced based on an ecological and simple approach via polymer crosslinking and casting techniques using a ternary crosslinked polymer containing poly (vinyl alcohol), poly (ethylene oxide) and poly (vinyl pyrrolidone) (Gouda et al., 2019) instead of benchmark Nafion® membranes. The polymer matrix doped with sulfonated graphene oxide (SGO) was used to enhance its mechanical properties and water retention of the membrane, whereas the sulfonic groups allowed keeping the membrane in a well-hydrated condition, thus improving the proton conductivity (Ayyaru and Ahn, 2017). However, to develop low-cost high-performance MEA, the fabrication procedures were tested using three types of MEAs and performance comparison was done to study the effect of gas diffusion layers (GDL) and the number of catalyst layers.

MATERIALS AND METHODS

Preparation of Electrode Materials

Preparation of Reduced Graphene Oxide (rGO)

Plastic bottles waste as sources of polyethylene terephthalate (PET) were used to prepare reduced graphene oxide (rGO). The PET bottle waste was ready to use as mentioned in a

previous study (El Essawy et al., 2017). Two grams of waste were introduced into an enclosed autoclave container and placed inside the center of an electric furnace at 800°C for 1 h. The resulting dark products were collected and crushed.

Preparation of Reduced Graphene Oxide/Magnetic Iron Oxide Nanocomposite (rGO/MIO)

rGO/MIO nanocomposite was synthesized by using an inverse co-precipitation process based on the precursors of ferric chloride ($FeCl_3.6H_2O$), ferrous sulfate ($FeSO_4.7H_2O$), and the precipitator of ammonium hydroxide (NH_4OH) (Ma et al., 2018). Twenty mL 0.2 M NH_4OH aqueous solution and 0.5 g of reduced graphene oxide (rGO) were added into a 250 mL four-neck bottle under N_2 atmosphere for 30 min and 1.08 g $FeCl_3.6H_2O$ and 0.54 g $FeSO_4.7H_2O$ with a stoichiometric ratio $[Fe^{2+}]$:$[Fe^{3+}]$ equal to 1:2, corresponding to Fe_3O_4, were dispersed using an ultrasonic dispersion method into 60 mL 1:1 (volume ratio) water-ethanol mixed solvents. The mixture was then poured rapidly into a four-neck bottle under vigorous mechanical stirring for 10 min with N_2 bubbling throughout the reaction. The nanocomposites were separated magnetically, washed with deionized water until the throwdown solution became neutral then dried in a vacuum oven at 80°C for 24 h.

Characterization of Electrode Materials

X-ray Diffraction (XRD) data (Shimadzu-7000, U.S.A.) was collected with a CuKα radiation beam (λ = 0.154060 nm). An X-ray Photoelectron Spectroscopy (XPS) Phi 5300 ESCA system (Perkin-Elmer, U.S.A) with Mg (Kα) radiation (X-ray energy 1253.6 eV) was used. A Transmission Electron Microscope (TEM) (TECNAI G20, Netherland with EDX) was also used. The Brunauer-Emmett-Teller (BET) surface area and total pore volume were measured using Barret-Joyner-Halenda (BJH) adsorption methods.

Electrochemical Measurements of Electrodes

The catalytic activity of rGO and rGO/MIO nanocomposites were tested for ORR in 0.1 M KOH electrolyte. The sample inks were prepared by ultrasonicating a mixture containing 450 µl of 2-propanol and 50 µl of 10 wt % Nafion mixture solution with 2.5 mg of sample to form a homogeneous ink. Then a polished and clean glassy carbon (GC) disk electrode with 0.126 cm^2 geometric surface area was loaded with 10 µL of suspension. Potentiostat/Galvanostatic (VoltaLab 40 PGZ301) with software Voltamaster4 was used for all electrochemical experiments.

The three-electrode electrochemical cell was used to conduct the electrochemical measurements at room temperature using 0.1 M KOH solution as the electrolyte. A graphite rod was used as the counter electrode, Hg/HgO (1 M NaOH) as a reference electrode and the tested prepared electrode material supported on GC as the working electrode. As electrode potentials presented in the manuscript refer to the Hg/HgO reference electrode. The electrolyte was saturated with N_2 or O_2 for 30 min before each electrochemical test.

Cyclic voltammetry (CV) was used to check the electrochemical activity of rGO or rGO/MIO in N_2-saturated electrolyte solution for three cycles with −0.8 V to 0.2 V potential window at 100 mVs^{-1} scan rate. Furthermore, the CV was also recorded in O_2-saturated electrolyte for three cycles with −0.8 V to 0.2 V potential window at 100 mVs^{-1} scan rate to investigate the initial behavior of the electrode.

To study the electrochemical kinetics, linear scan voltammetry with rotating disk electrode technique (LSV-RDE) was used in O_2-saturated alkaline electrolyte solution in the 0.2 to −0.8 V potential window at a scan rate of 5 mVs^{-1} under several rotation speeds while keeping the O_2 flow on the surface of the solution during the measurements. Koutecky–Levich equation (K-L equation) was used to determine the number of electrons involved in the electrochemical reactions as illustrated in Equations (1) and (2).

$$(1/j) = (1/j_k) + (1/j_d) = (1/j_k) + 1/(B\omega^{1/2}) \quad (1)$$

B was determined from the slope of the Koutecky-Levich plot according to Equation (2) given below,

$$B = 0.62\, n\, F\, C_{O2}\, D_{O2}{}^{2/3} \upsilon^{-1/6} \quad (2)$$

where j is the measured current density, j_k and j_d are the kinetic and diffusion limiting currents densities; respectively, ω is the speed of rotation in rpm, when the rotation speed is expressed in rpm the value of 0.62 is used, F is the Faraday constant (96,485 C mol^{-1}), D_{O2} is the oxygen diffusion coefficient in the alkaline electrolyte solution (1.9 × 10^{-5} cm^2 s^{-1}), υ is the kinematic viscosity (0.01 cm^2 s^{-1}), and C_{O2} is the oxygen concentration (0.0012 mol L^{-1}). Koutecky-Levich plot between *(1/j)* and $(\omega^{-1/2})$ was plotted to obtain the number of electrons transferred *(n)* from the slope and the kinetic-limiting current j_k from the intercept of the plot.

To determine the ionic conductivity of the prepared membrane and electrodes, resistance measurements were carried out by electrochemical impedance spectroscopy (EIS) technique at 5 mV in the frequency range of 0.1 Hz−500 kHz. The resistance is represented by the high-frequency intercept on the

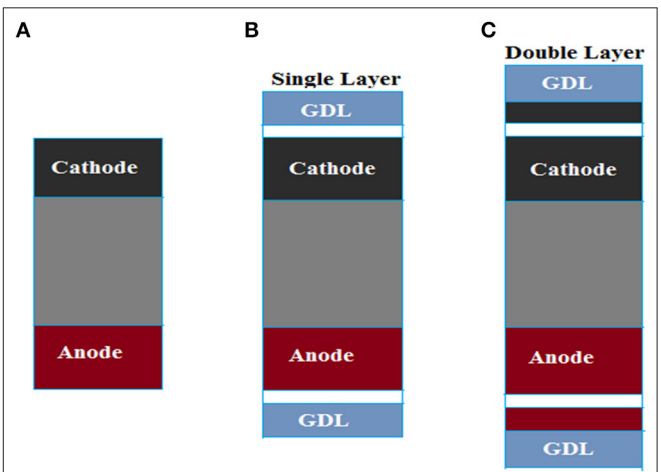

FIGURE 1 | Design of three membrane electrode assemblies (MEAs): **(A)** MEA 1, without GDL; **(B)** MEA 2, with single-layer electrodes; **(C)** MEA 3, with double-layer electrodes.

real axis of the complex impedance plot. The ionic conductivity was determined from resistance according to Equation (3),

$$\sigma = d/RA \quad (3)$$

where σ is the membrane ionic conductivity (S cm^{-1}), A is the geometric area (cm^2), d (cm) is the thickness and R (Ω) is the ohmic resistance.

Preparation and Characterization of PEM

The PVA/PEO/PVP blended polymers matrix named as PVA/PEO/PVP-SGO-3 was prepared and characterized as previously described (Gouda et al., 2019).

Preparation of Membrane Electrode Assembly

Spray method was used at the cathode and anode sides of the MEA. To identify an optimized fabrication concept, three types of MEAs were designed as depicted in **Figure 1** and the GDL used is carbon cloth (CeTech Carbon Cloth without MPL). The catalyst loading was adjusted to 0.4 mg cm^{-2} on anode and cathode. Both electrodes had an active surface area of 25 cm^2.

Cell Polarization Measurements

Polarization curves represent the trend of the losses affect PEM fuel cell performance. The single-cell was tested using Scribner Associates Model 850e test station. Fuel cell test station includes a computer-based control and data acquisition system based on advanced software for Electrochemical Research. The fuel cell polarization curves are obtained from this software whereas the voltage vs. current density of the fuel cell with model assumptions: an ideal mixture of reactant gasses, steady-state conditions, isothermal process, and fully hydrated system. In this study, polarization curves were monitored with potentiostatic mode for determining maximum and minimum potential and current values. After that polarization curves were recorded with galvanostatic mode (differential currents were chosen as 0.03 A at the low current region and 0.05 A at the high current region). In this way, most current values were obtained at the low current density. Humidified hydrogen and oxygen gases were fed to the fuel cell with the same flow rate of 250 sccm.

RESULTS AND DISCUSSION

Microscopic Visualization, Physical, and Chemical Characterizations of Electrodes Materials

As shown in **Figures 2A,B**, the TEM images of rGO and rGO/MIO nanocomposite demonstrate an exfoliated, crumpled and transparent flake-like morphology with several layers, in addition to entrapped iron oxide nanoparticles inside the graphene matrix for sample rGO/MIO and the EDX results implies presence of iron oxide in small ratio about 4% (atomic%) and that confirmed from the XPS results.

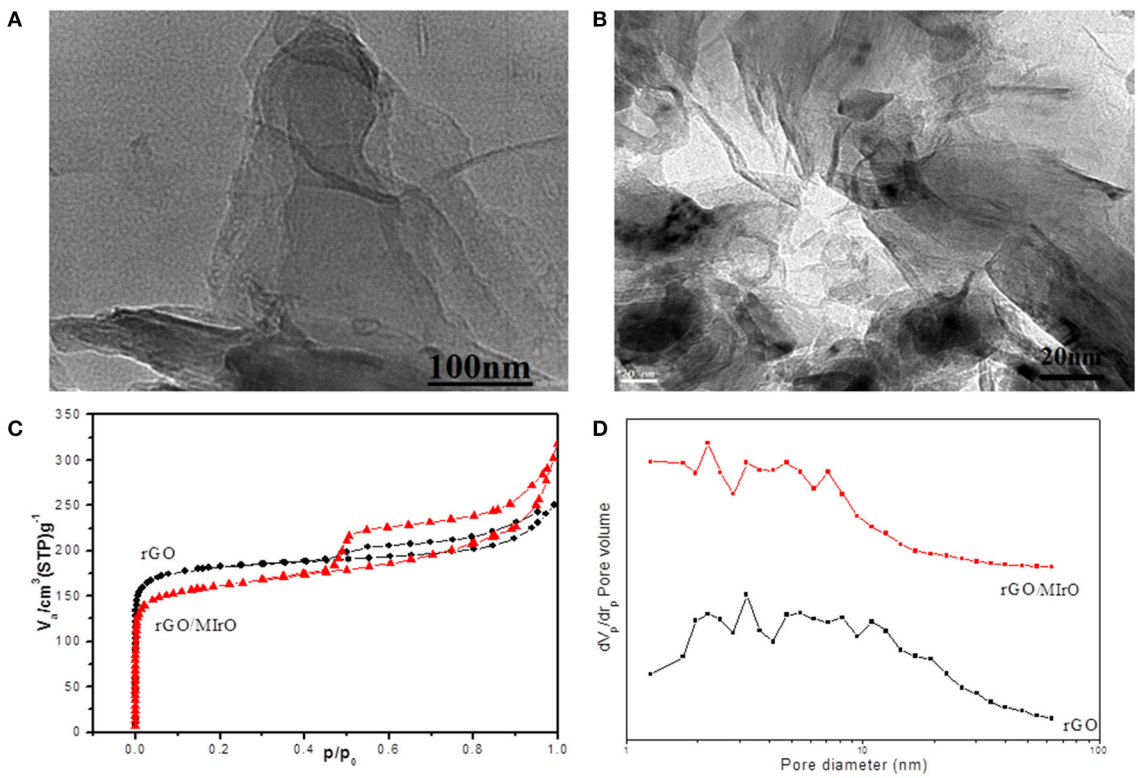

FIGURE 2 | TEM images for **(A)** rGO and **(B)** rGO/MIO samples. **(C)** N_2-adsorption-desorption isotherm and **(D)** BJH plot of rGO and rGO/MIO nanocomposite.

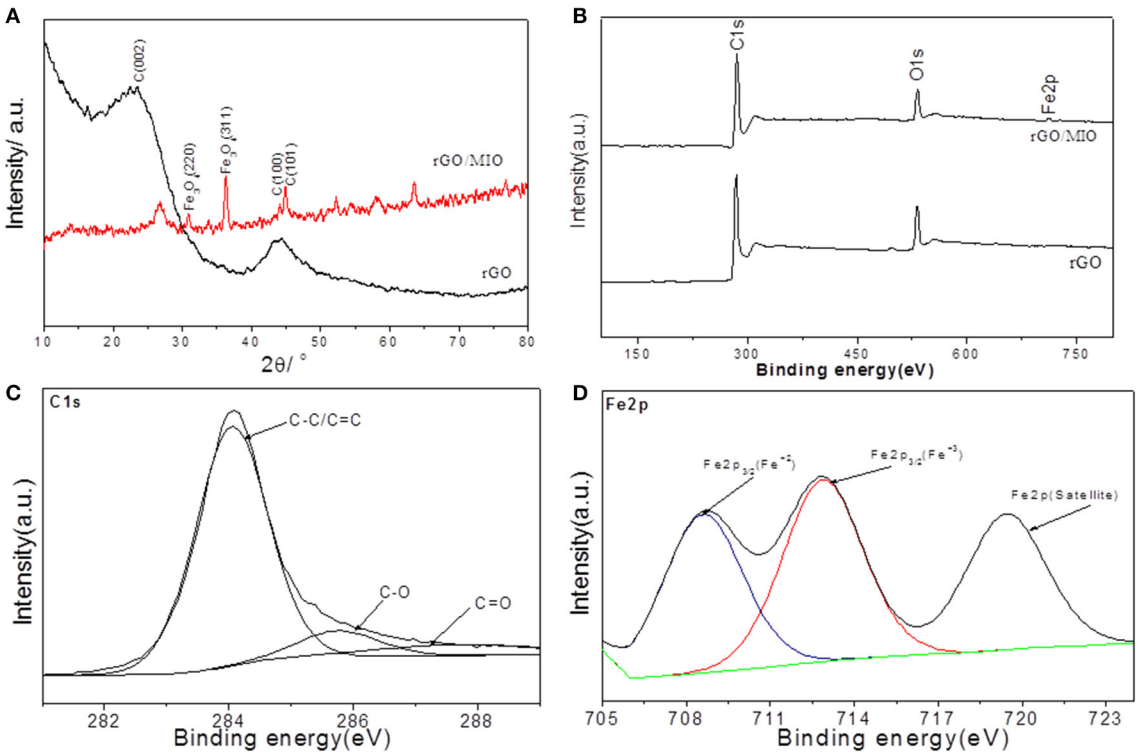

FIGURE 3 | (A) XRD patterns and **(B)** XPS survey spectra for rGO and rGO/MIO nanocomposite, together with high-resolution spectra of **(C)** C1s **(D)** Fe2p of rGO/MIO nanocomposite.

In order to investigate the surface porosity, an important factor affecting the mass transfer that affects the catalytic activity of the electrodes, the N_2 adsorption and desorption isotherm test at 77 K was performed. As can be seen in **Figure 2C**, rGO, and rGO/MIO nanocomposite samples presented isotherms with hysteresis loop of the Type IV, according to IUPAC classification, in the relative pressure range of 0.4–1.0, and capillary condensation, indicating the coexistence of microporous and mesoporous structure, as confirmed from BJH plot (**Figure 2D**) with mean pore diameter of 2.2 and 5.1 nm for rGO and rGO/MIO nanocomposite, respectively. However, it was noticed that the surface area and the pore size of rGO/MIO nanocomposite is higher than that of rGO indicating that, the introducing of iron oxide nanoparticles avoids the aggregation and restacking problems which led to an obvious increase in BET surface area and pore size and that is a valuable characteristic for electrocatalytic applications.

As can be seen in **Figure 3A** the XRD pattern of the rGO sample showed 2θ main peak at 26° and 44.3° which corresponds to the (002) and (100) reflections. For rGO/MIO sample, a slight shift for (002) plane was due to introducing of Fe_3O_4 nanoparticles between the rGO nanosheets thus increasing the interlayer spacing and that is beneficial to promote charge transfer in electrodes materials. However, the peaks at 2θ values of 30.28 (220) and 35.78 (311) are in good agreement with the inverse cubic spinel phase of Fe_3O_4 (ICDD card no.01-07-5088).

To explore the graphitic content and carbon speciation in rGO and rGO/MIO samples, X-ray photoelectron spectroscopy (XPS) was used. As shown in **Figure 3B**, the obtained material was formed with a high amount of carbon and a low amount of oxygen, in addition to traces of iron for rGO/MIO sample. The chemical bonding composition of rGO/MIO nanocomposite was investigated as shown in the high-resolution C1s and Fe2p spectra (**Figures 3C,D**). The peak in C1s at 284.19 eV corresponding to sp^2-hybridization (C-C bond and C=C), demonstrates that most of the C atoms are arranged in a honeycomb lattice, and the fitted peaks centered at 285.87 and 287.88 eV are assigned to C-O and C=O respectively. The Fe2p spectra reveal the presence of two components assigned to Fe^{2+} and Fe^{3+} oxides, where Fe^{3+} is the dominant component. Only $Fe2p_{3/2}$ is represented due to overlapping occurring between $2p_{3/2}$ and $2p_{1/2}$ edges (Otero et al., 2008; Molchan et al., 2015).

Half Cell Electrochemical Measurements

rGO and rGO/MIO samples were prepared from one-step thermal dissociation process of PET waste and have two-dimensional mesoporous structures with large surface area, pore volume, and pore size, being appropriate for electrocatalytic applications. To evaluate the ability of using prepared rGO and rGO/MIO as electrocatalysts in fuel cell application, the electrocatalytic activity of the prepared electrodes toward ORR was evaluated using cyclic voltammetry (CV), linear

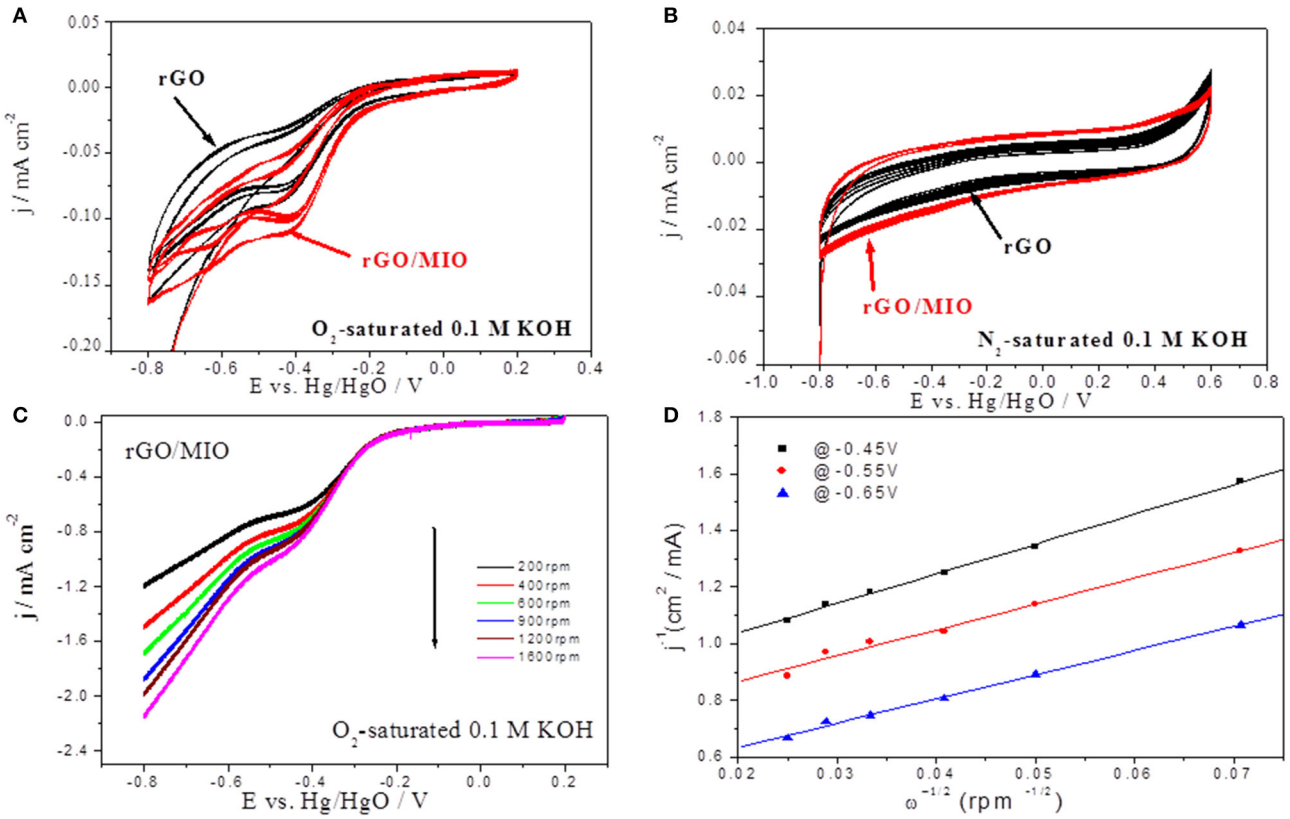

FIGURE 4 | CVs run at 100 mVs^{-1} with rGO and rGO/MIO electrodes in **(A)** O_2-saturated and **(B)** N_2-saturated 0.1 M KOH section. **(C)** Linear scan voltammograms recorded in O_2-saturated 0.1 M KOH at 5 mV s^{-1} and different rotation rates for ORR on rGO/MIO and **(D)** the corresponding Koutecky-Levich Plot obtained at three different potentials.

scan voltammetry (LSV) combined with rotating disk electrode (RDE) technique and electrochemical impedance spectroscopy (EIS).

The CV curves of both samples in O_2-saturated 0.1 M KOH electrolytes are shown in **Figure 4A**, where both samples showed cathodic current peaks. It is noticeable that the rGO/MIO sample has earlier onset potential than the rGO sample, in addition to higher reduction current density, suggesting higher ORR activity of rGO/MIO. **Figure 4B** shows the CVs of both samples in N_2 saturated 0.1M KOH electrolyte with the two samples showing similar behavior. From the previous CV survey, the prepared RGO material was selected to be used as the fuel cell anode and rGO/MIO was selected as the cathode material.

The ORR kinetics of the prepared rGO/MIO catalyst electrode were further studied by the LSV-RDE technique in O_2- saturated 0.1 M KOH electrolyte at different rotation rates (200, 400, 600, 900, 1,200, 1,600 rpm). As shown in **Figure 4C**, LSV curves confirmed its electrocatalytic performance in almost one-step process with an onset potential of ca. −0.25 V and the diffusion current increased with the increasing of the rotation rate which confirm that the reaction is diffusion-controlled under the tested condition. Moreover, three regions of interest can be distinguished, namely, the diffusion-controlled region at potential $E < -0.3$ V, the mixed diffusion kinetic region at potential $-0.1 \geq E \geq -0.3$ V, and the kinetics controlled region at $E \geq -0.1$ V. To calculate the number of electrons transferred during ORR, the Koutecky–Levich plots (K-L plot) at different potentials (−0.45 V, −0.55 V, and −0.65 V) were plotted (**Figure 4D**) and the average electron number was calculated. A value of about four electrons was found, suggesting a direct four-electron pathway for ORR ($O_2 + 4H^+ + 4e^- \rightarrow 2H_2O$), being this path the preferred (and more favorable) for fuel cell processes (Zhang et al., 2015).

It is known that electrochemical impedance spectroscopy (EIS) allows estimating ionic and electric conductivity of different systems. It is accepted that the high-frequency region of an impedance spectrum is associated with the internal ohmic resistance and the contact capacitance in the granular electrode structure, whereas the medium and low-frequency regions represent the charge-transfer resistance and the mass transport resistance, respectively (Yuan et al., 2010).

As shown in **Figures 5A,C,E** the incomplete semicircle that is potential independent has been assigned to different features, namely to internal ohmic resistance (R_{ohm}), represented by high-frequency intersection of the semicircle with the x-axis, charge-transfer resistance (R_{ct}), represented by the diameter of the semicircle, and contact capacitance in the granular electrode structure, represented by straight line at the high-frequency end of the semicircle (Fischer et al., 1998). As for the incomplete semicircle, it refers to a distributed resistance effect (Paganin

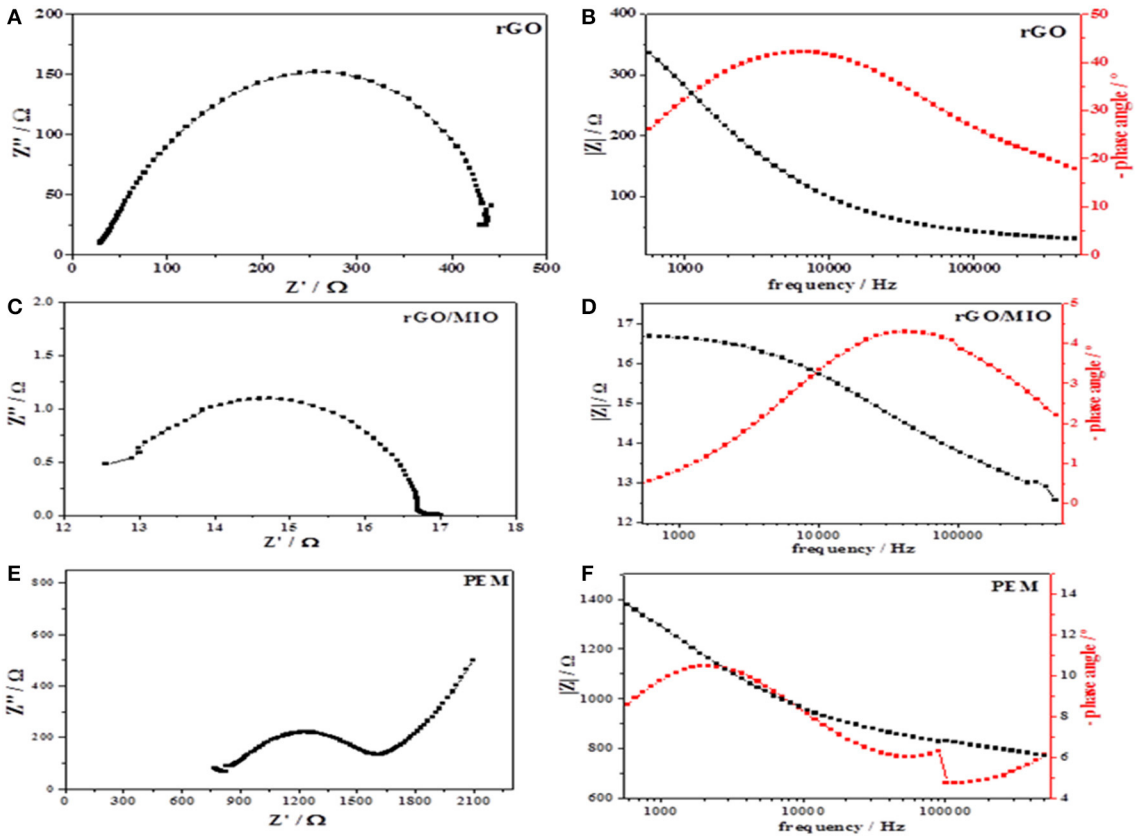

FIGURE 5 | Nyquist **(A,C,E)** and Bode **(B,D,F)** plots obtained for the rGO anode, the rGO/MIO cathode and for the PEM fuel cell.

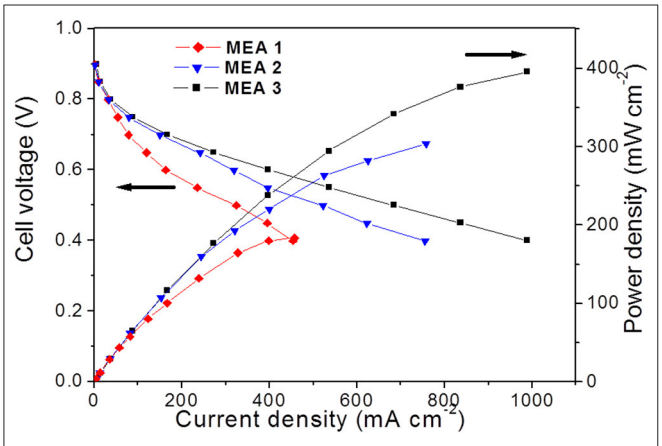

FIGURE 6 | Polarization **(Left)** and power density **(Right)** curves for the 3 designed MEAs. MEA1 contains single-layer electrodes without GDL, MEA2 contains single-layer electrodes with GDL and MEA3 contains double-layer electrodes.

et al., 1998). From Nyquist plots, the calculated ionic conductivity of anode (rGO), cathode (rGO/MIO) and PEM are 0.3, 7, and 0.07 mS cm^{-1} respectively. Furthermore, the Nyquist semicircle of the rGO/MIO sample is smaller than that of the rGO sample, indicating that it has lower resistance and better charge transfer. However, the main reasons for the higher conductivity (lower resistance) of rGO/MIO nanocomposite (than the original rGO sample) could be attributed to the following points: (i) the introduction of iron oxide nanoparticles slightly increased the degree of graphitization, which is beneficial for promoting the charge transfer (Liu et al., 2019a) (2) and (ii) iron oxide nanoparticles accelerate the electron transfer, which in turn enhances the conductivity of the rGO/MIO nanocomposite (Yang et al., 2017). In addition, the relaxation time peak from Bode plot (**Figures 5B,D**) is not well clear. However, this is favorable for the cathode material in fuel cells (Qayyum et al., 2016). On the other side, for rGO sample the Nyquist semicircle at low frequency characterized by higher polarization resistance more than rGO/MIO and that is a characteristic property for anode material (Siracusano et al., 2018). An incomplete semicircle ended with a straight line in the high-frequency range was detected for PEM as shown in **Figure 5E** and that attributed to the membrane characteristic property, however the Bode plot shown in **Figure 5F** exhibits two time constants at high frequencies and that is related to the membrane structure (Zhao-Luo et al., 2018).

Cell Performance

In general, MEA fabrication can come from two techniques. The first one is based on spraying the catalyst ink directly

onto the membrane, followed by a hot pressing step, while in the second technique the catalyst ink is directly sprayed onto the GDL and then hot-pressed onto the membrane (Frey and Linardi, 2004; Kim et al., 2015). The advantage of these techniques is that the catalyst loading can be adjusted by simply weighing the MEA or the GDL before and after coating with the catalyst ink but there is a risk of irregular catalyst transfer from the transfer film to the membrane. For that reason, an investigation on a cell performance of the developed MEA fabrication technique combining effect of using GDL and number of CLs was conducted using single-cell measurements with H_2/O_2 operation, however only easy steps were chosen in this preparation technique without using assembly hot pressing in order to simplify the method and reduce the production cost with regard to maximal performance in addition to, preventing a distortion in the pore structures of catalyst layers and gas diffusion layers.

Figure 6 shows the performance and power densities of the fabricated MEA 1, MEA 2 and MEA 3, whereas the lowest performance was for MEA 1, which was fabricated by using catalyst-coated membrane technique without GDL, compared to MEA 2, which was fabricated by using the same technique but using carbon cloth without a microporous layer as GDL. The addition of GDL to MEA facilitates the transport of interrupted gas and formed water through the electrochemically active areas of the MEA (Omrani and Shabani, 2017). It also prevents leakage of the electrode material throughout the MEA, thus leading to a performance enhancement of MEA 2 of 66% when compared to MEA 1.

The effect of the number of CLs also affects the performance of fabricated MEA 2 and MEA 3 examined and compared here. The electrode ink was sprayed onto the membrane only as in MEA 2 and onto the GDL and the membrane as in MEA 3. The results show that the highest power densities up to 395 $mWcm^{-2}$ at 988 mA cm^{-2} can be produced from MEA 3 with GDL and double-layered electrodes. Consequently, this result confirms the MEA performance depends on the electrode CLs number and morphology, and that could be referred to increasing the mass transport through the double layer electrodes, in addition to providing an effective path channel for water removal through the larger pores of the high porosity CL coated onto GDL.

CONCLUSIONS

This work contributes toward sustainable materials processing with upcycling technology to produce highly added-value products from reduced graphene oxide and reduced graphene oxide/magnetic iron oxide nanocomposite, produced from the thermal dissociation of plastic waste using simple, one-pot and applicable method. The prepared materials can be used as active catalyst electrodes with high durability for ORR in fuel cells, and hence get the benefits of simultaneous waste management and increasing the possibility for commercialization of low-temperature fuel cells by decreasing its production cost. Moreover, to develop high-performance MEAs and to identify the optimum fabrication conditions, three types of MEAs were designed. The optimum one is the MEA designed with a double-layer electrode involving an inner catalyst layer prepared by the catalyst-coated membrane (CCM) method and an outer catalyst layer directly coated on the gas diffusion layer to increase the catalyst utilization. Further investigations need to be carried out to elucidate the effect of using GDLs with a microporous layer on the performance of MEAs obtained in combination with the followed preparation technique.

DATA AVAILABILITY STATEMENT

All datasets generated for this study are included in the article.

AUTHOR CONTRIBUTIONS

MG fabricated the PEM and MEA. ME also participated in MEA fabrication, carried out CV and impedance measurements, and analyzed the experimental data. AA and MY performed and analyzed the data of fuel cell test station for fabricated MEAs. DS supervised and revised the manuscript. NE proposed the project, carried out electrodes preparation and characterization, and wrote the manuscript with input from the other coauthors.

FUNDING

DS would like to thank Fundação para a Ciência e a Tecnologia (FCT, Portugal) for contract no. IF/01084/2014/CP1214/CT0003 under IF2014 Programme.

REFERENCES

Awang, N., Ismail, A. F., Jaafar, J., Matsuura, T., Junoh, H., Othman, M. H. D., et al. (2015). Functionalization of polymeric materials as a high performance membrane for direct methanol fuel cell: a review. *React. Funct. Polym.* 86, 248–258. doi: 10.1016/j.reactfunctpolym.2014.09.019

Ayyaru, S., and Ahn, Y. (2017). Application of sulfonic acid group functionalized graphene oxide to improve hydrophilicity, permeability, and antifouling of PVDF nanocomposite ultrafiltration membranes. *J. Membr. Sci.* 525, 210–219. doi: 10.1016/j.memsci.2016.10.048

Aziz, A. N., Hassab, M. A., Elsayed Youssef, M., and El-Maghlany, W. M. (2018). "Performance analysis of DMFC and PEMFC numerically with models validation," in *International Journal of Advances in Electronics and Computer Science* 5, 14–17.

Bakangura, E., Wu, L., Ge, L., Yang, Z., and Xu, T. (2016). Mixed matrix proton exchange membranes for fuel cells: state of the art and perspectives. *Prog. Polym. Sci.* 57,103–152. doi: 10.1016/j.progpolymsci.2015.11.004

Beydaghi, H., Javanbakht, M., and Kowsari, E. (2014). Synthesis and characterization of poly (vinyl alcohol)/sulfonated graphene oxide nanocomposite membranes for use in proton exchange membrane fuel cells (PEMFCs). *Ind. Eng. Chem. Res.* 53, 16621–16632. doi: 10.1021/ie502491d

Choi, H., Kumar, N. A., and Baek, J. (2015). Graphene supported non-precious metal-macrocycle catalysts for oxygen reduction reaction in fuel cells. *Nanoscale* 7, 6991–6998. doi: 10.1039/C4NR06831A

Dumont, J. H., Martinez, U., Artyushkova, K., Purdy, G. M., Dattelbaum, A. M., Zelenay, P., et al. (2019). Nitrogen-doped graphene oxide electrocatalysts for the oxygen reduction reaction. *ACS Appl. Nano Mater.* 2, 1675–1682. doi: 10.1021/acsanm.8b02235

El Essawy, N. A., Konsowa, A. H., Elnouby, M., and Farag, H. A. (2017). A novel one-step synthesis for carbon-based nanomaterials from polyethylene

terephthalate (PET) bottles waste. *J. Air Waste Manage. Assoc*. 67, 358–370. doi: 10.1080/10962247.2016.1242517

Fischer, A., Jindra, J., and Wendt, H. (1998). Porosity and catalyst utilization of thin layer cathodes in air operated PEM-fuel cells. *J. Appl. Electrochem*. 28, 277–282. doi: 10.1023/A:1003259531775

Frey, T., and Linardi, M. (2004). Effects of membrane electrode assembly preparation on the polymer electrolyte membrane fuel cell performance. *Electrochim. Acta* 50, 99–105. doi: 10.1016/j.electacta.2004.07.017

Gao, S., Fan, B., Feng, R., Ye, C., Wei, X., Xu, J., et al. (2017). N-doped-carbon-coated Fe_3O_4 from metal-organic framework as efficient electrocatalyst for ORR. *Nano Energy* 40, 462–470. doi: 10.1016/j.nanoen.2017.08.044

Gouda, M. H., Gouveia, W., Afonso, M. L., Šljukić, B., El Essawy, N. A., Nassr, A. B. A. A., et al. (2019). Poly(vinyl alcohol)-based crosslinked ternary polymer blend doped with sulfonated graphene oxide as a sustainable composite membrane for direct borohydride fuel cells. *J. Power Sources* 432, 92–101. doi: 10.1016/j.jpowsour.2019.05.078

Gupta, S., Kellogg, W., Xu, H., Liu, X., Cho, J., and Wu, G. (2016). Bifunctional perovskite oxide catalysts for oxygen reduction and evolution in alkaline media. *Chem. Asian J.* 11, 10–21. doi: 10.1002/asia.201500640

Iwan, A., Malinowski, M., and Pasciak, G. (2015). Polymer fuel cell components modified by graphene: electrodes, electrolytes and bipolar plates. *Renew. Sustain. Energy Rev*. 49, 954–967. doi: 10.1016/j.rser.2015.04.093

Kim, G., Eom, K., Kim, M., Yoo, S., Jang, J., Kim, H., et al. (2015). Design of an advanced membrane electrode assembly employing a double-layered cathode for a PEM fuel cell. *ACS Appl. Mater. Interfaces* 7, 27581–27585. doi: 10.1021/acsami.5b07346

Lai, Q., Zheng, L., Liang, Y., He, J., Zhao, J., and Chen, J. (2017). Metal–organic-framework-derived Fe-N/C electrocatalyst with five-coordinated Fe-Nx sites for advanced oxygen reduction in acid media. *ACS Catal.* 7, 1655–1663. doi: 10.1021/acscatal.6b02966

Li, C., Xiao, L., Jiang, Z., Tian, X., Luo, L., Liu, W., et al. (2017). Sulfonic acid functionalized graphene oxide paper sandwiched in sulfonated poly(ether ether ketone): a proton exchange membrane with high performance for semipassive direct methanol fuel cells. *Int. J. Hydrog. Energy*. 42,16731–16740. doi: 10.1016/j.ijhydene.2017.05.126

Liu, M., Guo, X., Hu, L., Yuan, H., Wang, G., Dai, B., et al. (2019a). Fe_3O_4/Fe_3C@nitrogen-doped carbon for enhancing oxygen reduction reaction. *Chem. Nano. Mat*. 5:138. doi: 10.1002/cnma.201800594

Liu, M., Zhao, Z., Duan, X., and Huang, Y. (2019b). Nanoscale structure design for high-performance Pt-based ORR catalysts. *Adv. Mater*. 31:1802234. doi: 10.1002/adma.201802234

Ma, Y., Jin, P., Lei, W., La, P., Du, X., and Zhang, D. (2018). One-pot method fabrication of superparamagnetic sulfonated polystyrene/Fe_3O_4/graphene oxide micro-nano composites. *J Porous Mater*. 25, 1447–1453. doi: 10.1007/s10934-018-0557-8

Molchan, I. S., Thompson, G. E., Skeldon, P., Lindsay, R., Walton, J., Kouvelos, E., et al. (2015). Microscopic study of the corrosion behaviour of mild steel in ionic liquids for CO_2 capture applications. *RSC Adv*. 5, 35181–35194. doi: 10.1039/C5RA01097G

Morales-Acosta, D., Flores-Oyervides, J. D., Rodríguez-González, J. A., Sánchez-Padilla, N. M., Benavides, R., et al. (2019). Comparative methods for reduction and sulfonation of graphene oxide for fuel cell electrode applications. *Int. J. Hydrog. Energy* 44, 12356–12364. doi: 10.1016/j.ijhydene.2019.02.091

Omrani, R., and Shabani, B. (2017). Gas diffusion layer modifications and treatments for improving the performance of proton exchange membrane fuel cells and electrolysers: a review. *Int. J. Hydrog. Energy* 42, 28515–28536. doi.org/10.1016/j.ijhydene.2017.09.132

Otero, E., Wilks, R. G., Regier, T., Blyth, R. I., Moewes, A., and Urquhart, S. G. (2008). Substituent effects in the iron 2p and carbon 1s Edge Near-Edge X-ray Absorption Fine Structure (NEXAFS) spectroscopy of ferrocene compounds. *J. Phys. Chem. A* 112, 624–634. doi: 10.1021/jp074625w

Paganin,V. A., Oliveira, C. L. F., Ticianelli, E. A., Springer, T. E., and Gonzalez, E. R. (1998). Modelistic interpretation of the impedance response of a polymer electrolyte fuel cell. *Electrochim. Acta* 43, 3761–3766. doi: 10.1016/S0013-4686(98)00135-2

Pandey, R. P., Shukla, G., Manohar, M., and Shahi, V. K. (2017). Graphene oxide based nanohybrid proton exchange membranes for fuel cell applications: an overview. *Adv. Colloid Interface Sci*. 240, 15–30. doi: 10.1016/j.cis.2016.12.003

Pourzare, K., Mansourpanah, Y., and Farhadi, S. (2016). Advanced nanocomposite membranes for fuel cell applications: a comprehensive review. *Biofuel Res. J*. 12, 496–513. doi: 10.18331/BRJ2016.3.4.4

Qayyum, H., Tseng, C.-J., Huang, T.-W., and Chen, S.-Y. (2016). Pulsed laser deposition of platinum nanoparticles as a catalyst for high-performance PEM fuel cells. *Catalysts* 6:180. doi: 10.3390/catal6110180

Qiu, X., Dong, T., Ueda, M., Zhang, X., and Wang, L. (2017). Sulfonated reduced graphene oxide as a conductive layer in sulfonated poly(ether ether ketone) nanocomposite membranes. *J. Membr. Sci*. 524, 663–672. doi: 10.1016/j.memsci.2016.11.064

Sedesheva, Y. S., Ivanov, V. S., Wozniak, A. I., and Yegorov, A. S. (2016). Proton-exchange membranes based on sulfonated polymers, Orient. *J. Chem*. 32, 2283–2296. doi: 10.13005/ojc/320501

Shen, A., Zou, Y., Wang, Q., Dryfe, R. A. W., Huang, X., Dou, S., et al. (2014). Oxygen reduction reaction in a droplet on graphite: direct evidence that the edge is more active than the basal plane. *Angew. Chem. Int. Ed*. 53, 1–6. doi: 10.1002/anie.201406695

Siracusano, S., Trocino, S., Briguglio, N., Baglio, V., and Aricò, A. S. (2018). Electrochemical impedance spectroscopy as a diagnostic tool in polymer electrolyte membrane electrolysis. *Materials* 11:1368. doi: 10.3390/ma11081368

Su, Y., Jiang, H., Zhu, Y., Zou, W., Yang, X., Chen, J., et al. (2014). Hierarchical porous iron and nitrogen co-doped carbons as efficient oxygen reduction electrocatalysts in neutral media. *J. Power Source* 265, 246–253. doi: 10.1016/j.jpowsour.2014.04.140

Thanasilp, S., and Hunsom, M. (2010). Effect of MEA fabrication techniques on the cell performance of Pt–Pd/C electrocatalyst for oxygen reduction in PEM fuel cell. *Fuel* 89, 3847–3852. doi: 10.1016/j.fuel.2010.07.008

Yang, J., Hu, J., Weng, M., Tan, R., Tian, L., Yang, J., et al. (2017). Fe-cluster pushing electrons to n-doped graphitic layers with Fe_3C(Fe) hybrid nanostructure to enhance O_2 reduction catalysis of Zn-air batteries. *ACS Appl. Mater. Interfaces* 9, 4587–4596. doi: 10.1021/acsami.6b13166

Ye, L., Chai, G., and Wen, Z. (2017). Zn-MOF-74 derived N-doped mesoporous carbon as pH-universal electrocatalyst for oxygen reduction reaction. *Adv. Funct. Mater.* 27:1606190. doi: 10.1002/adfm.201606190

Yuan, X.-Z., Song, C., Wang, H., and Zhang, J. (2010). "EIS diagnosis for PEM fuel cell performance," in *Electrochemical Impedance Spectroscopy in PEM Fuel Cells* (London: Springer), 193–262. doi: 10.1007/978-1-84882-846-9

Zhang, J., Zhao, Z., Xia, Z., and Dai, L. (2015). A metal-free bifunctional electrocatalyst for oxygen reduction and oxygen evolution reactions. *Nat. Nanotechnol*. 10, 444–453. doi: 10.1038/nnano.2015.48

Zhao-Luo, Q., Huang, Q., Chen, Z., Yao, L., Fu, P., and Lin, Z. (2018). Polyvinylidene fluoride membranes probed by electrochemical impedance spectroscopy. *Mater. Res. Express* 5:065507. doi: 10.1088/2053-1591/aac7f2

Conflict of Interest: The authors declare that the research was conducted in the absence of any commercial or financial relationships that could be construed as a potential conflict of interest.